Tropical Convective Cloud Characterization Using Ground-Based Microwave Radiometric Observations

R. Renju, C. Suresh Raju, Nizy Mathew, N. V. P. Kirankumar, and K. Krishna Moorthy

***Abstract*—Characterization of the microphysical and thermodynamical properties of convective events over the tropical coastal station Thiruvananthapuram (TVM) has been carried out based on multiyear microwave radiometer profiler observations. The analyses have been extended to develop a methodology to identify convective events, which is based on the radiometric brightness temperature (T_b) difference threshold, at 30 and 22.23 GHz channels, and the results are compared with reflectivity and rainfall intensity deduced from concurrent and collocated disdrometer measurements. Eighty-four of such convections were identified using the aforementioned methodology over the station during 2010–2013, i.e., both for pre- and post-Indian summer monsoon months, and further evaluated by computing their stability indexes. The occurrence of convective systems peaks in the afternoon and early-morning hours with genesis, respectively, over the land and the sea.**

***Index Terms*—Brightness temperature, convective systems (CSs), microwave radiometer.**

I. Introduction

THE characterization of convective systems (CSs) in the tropics is of fundamental importance in understanding the weather and climate of the Earth, as these are linked to the energy budget and water cycle through precipitation. The large latent heat release associated with the strong convective precipitation heats the troposphere, and the anvils influence the synoptic and mesoscale radiation balance [1], [2]. The high frequency of occurrences, large vertical extent, and the large amount of heat and moisture transported by these systems play important roles in the dynamics of tropical disturbances and the general circulation [3]. The CSs are classified according to their size, vertical extent, lifetime, and other related features, such as short-lived single cell, the discretely propagating multicells, and the long-lived continuously propagating supercells. Characterization of CSs is carried out remotely in terms of microwave brightness temperatures (T_b), cloud top infrared irradiance, and radar reflectivity, which are measured both from spaceborne and ground-based platforms. The relatively short lifetimes (of a few hours) and the small horizontal scales of the convective clouds make it difficult to observe them directly from satellite observations, and in such occasions, the ground-based observations play a pivotal role.

The organized mesoscale CSs (MCSs) are a combination of both convective and stratiform cloud regimes [4]. The convective regimes range from a few kilometers to ∼30 km in scale size (horizontal), with numerous deep cells having strong updrafts and downdrafts with heavy precipitation, while the stratiform regimes extend horizontally for hundreds of kilometers and generally cause low rain rates [5]. The knowledge of rainfall associated with stratiform or convective clouds is important in observational, modeling, and remote sensing studies since the microphysical processes are different for these cloud types [6]. Several methods have been developed for discriminating convective and stratiform cloud regions of MCSs. The bright band in radar, which occurs for stratiform clouds, and the echo intensity of 38 dBZ are the criteria to distinguish between the two precipitation types. Usually, convective precipitations are characterized with the large rain drops and stratiform precipitations with the smaller drops [9]. The transition region between the convective and stratiform, which is similar to the class mixed convective/stratiform, has been also observed [10], where both convective and stratiform points overlap, and distinguishing between them is difficult.

Thiruvananthapuram (TVM) is a near-equatorial coastal station (8.5° N, 76.9° E), and it experiences tropical weather with a moderate temperature regulated by the adjoining sea. The hot and humid conditions prevailing during March to May and October to November are very conducive for the formation of local deep convection and MCSs. These CSs are the major sources of the significant rainfall over this region (∼45% of the annual precipitation). However, studies leading to the understanding of the evolution and thermodynamical characteristics of the CSs over this region are highly limited. The diurnal variability of water vapor during the pre-monsoon is mainly attributed to the CSs [11].

A multifrequency microwave radiometer profiler (MRP, model: MP-3000A) has been operational at TVM since April 2010 for continuous measurements of atmospheric parameters with high temporal (∼1 min) and vertical (50–250 m) resolutions. The MRP is aligned in the north–south direction, which is parallel to the coastline of the Arabian Sea. It scans in the east–west direction, observing the atmosphere over the land in the east scan and over the sea in the west scan, thereby providing a unique opportunity to study the CSs over the two contrasting surfaces. The potential of microwave radiometer to study the genesis and evolution of local convective events and the formation of waterspout over this station was demonstrated [12].

Manuscript received October 29, 2015; revised January 13, 2016; accepted January 23, 2016. Date of publication March 1, 2016; date of current version May 24, 2016.

R. Renju, C. Suresh Raju, N. Mathew, and N. V. P. Kirankumar are with the Space Physics Laboratory, Vikram Sarabhai Space Centre, Indian Space Research Organisation, Trivandrum 695022, India (e-mail: c_sureshraju@vssc.gov.in).

K. Krishna Moorthy is with Indian Space Research Organisation Head Quarters, Bengaluru 560231, India.

Color versions of one or more of the figures in this paper are available online at http://ieeexplore.ieee.org.

Digital Object Identifier 10.1109/TGRS.2016.2527099

In this paper, four years of the MRP data (2010–2013) during both pre-monsoon (January–May) and post-monsoon (October–December) months have been analyzed 1) to develop a methodology to identify the CSs, using T_b values at 22.23 GHz and 30 GHz; 2) to characterize the types of CSs over this region, in terms of their genesis, evolution, and propagation; and 3) to understand the manner in which deep convection interacts with the large-scale environment.

II. Instruments and Data

A. MRP

The MRP measures T_b values through a sequential scan of 8 frequencies in the K-band (22.23–30.0 GHz) and 14 in the V-band (51.2–58.8 GHz). The bandwidth for each channel is 300 MHz. The beamwidth is 5°–6° at 22–30 GHz and 2°–3° at 51–59 GHz. A zenith-looking infrared (IR) radiometer and a rain detector are also attached to the profiler for estimating the cloud base height (CBH) and rain information, respectively. The K-band channels are calibrated to 0.3 K RMS by automated tipping procedures, and V-band channels are calibrated to 0.5 K RMS with a liquid nitrogen target [13]. As the ground-based microwave radiometric profiling is free from surface emissions, estimates of atmospheric temperature and humidity in the lower atmospheric region are accurate, and it is effective for a wide range of atmospheric and meteorological conditions [14]. The MRP is set to a multiangle scan mode in the east–west direction at an elevated plane, where it measures the multichannel T_b at seven fixed elevation angles, such as 15°, 30°, 45° over the land, 90° at zenith, and 135°, 150°, 165° over the sea. It permits the observation of propagation of CSs to sea, which are having genesis over the land and vice versa. The technical details of the profiler are available in [15] and also online (www.radiometrics.com).

B. Disdrometer

A Joss–Waldvogel disdrometer is an impact-type disdrometer that measures the drop sizes continuously at the MRP site. The sensor has a sampling cross-sectional area of 50 cm^2 and sorts drops into 20 size intervals ranging from 0.3–5.0 mm with an accuracy of 5%. The data are sampled at 1-min intervals. The integral parameter rain rate R (mm $\cdot$ h^{-1}) and the reflectivity Z (dBZ) are estimated from the quality-controlled drop spectra. The disdrometer rain rate measurements over this station are validated by comparing with the measurements from the collocated tipping bucket rain gauge, which yielded the correlation coefficient of 0.98 [16].

III. Results and Discussion

1) MRP Response to CSs: Different organized forms of deep convection are known as convective modes; each of them has different dynamics and meteorological setting, characterized by a specific combination of latent instability and vertical wind shear. These convective modes include single cells, multicells, and supercells. Short-lived single cells occur in an environment of low vertical wind shear. A multicell convection consists of multiple convective updrafts and downdrafts by the development of new convective cells along the boundary of the cold pool originating from an older cell. The supercell convections, which have a longer lifetime, are known for producing severe weather. During convection, the T_b values of K-band channel show large variability, particularly the 30 GHz, depending on the microphysical variability, as it is sensitive to cloud liquid water [12]. Hence, to account for the enhancement in the T_b values, the difference between the T_b values during the convection period and during the prevailing atmospheric condition (δT_b) has been estimated. The variability of δT_b, for all K-band channels, during three different types of convections, i.e., "a single cell occurred on February 22, 2011; multicell on April 03, 2011 and supercell on November 25, 2013," observed by MRP is shown in Fig. 1, and the rainfall durations over the station during these events are marked in black vertical lines. The 30 GHz channel shows maximum variability with large enhancement during the convection, and δT_b reaches up to $\sim$180 K. In the case of multicell formation (middle panel), the δT_b values are falling up to $\sim$50 K along the boundaries. During November 25, this δT_b persists for a longer period ($>$ 4 h), indicating the formation of supercells over the study region (third panel). Thus, temporal δT_b variation manifests the signature of different convective modes. In addition, δT_b variability of the 58.8 GHz channel shows negative values during the rain period, which is attributed to cooling of the surface and lower atmospheric region by the cold downdraft.

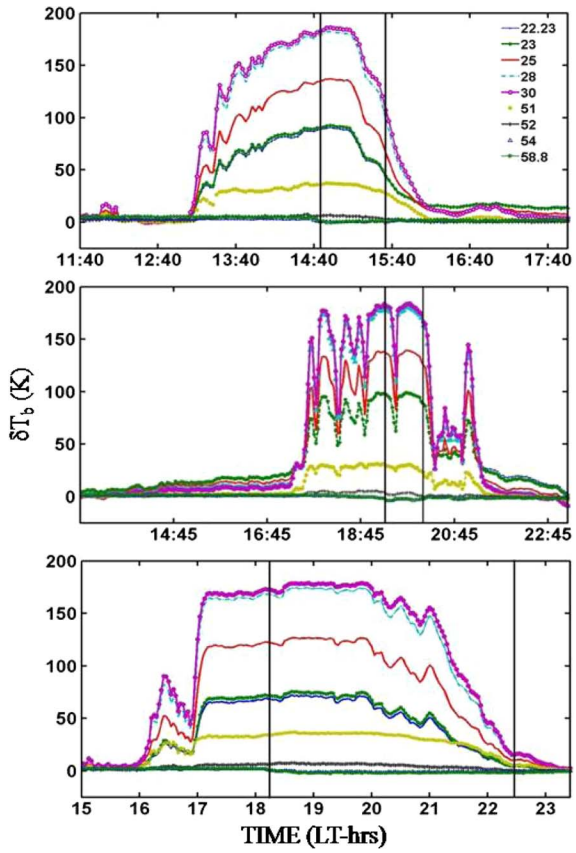

Fig. 1. Brightness temperature difference (δT_b (K)) of MRP channels for single-cell, multicell, and supercell MCS events, with black vertical lines indicating the duration of rainfall during the event over the site.

2) Humidity Variation and Propagation of an MCS: The MRP allows the continuous observation of thermal evolution

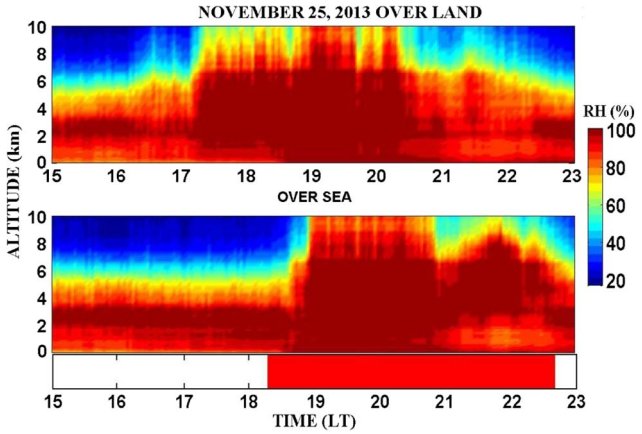

Fig. 2. Temporal evolution of the vertical distribution of RH during the supercell on November 25, 2013: (top panel) over land (15° elevation angle) and (bottom panel) over the sea (165° elevation angle). The period of rainfall is shown in the bottom panel observed by the rain sensor (rain flag is marked 1 when rainfall is present and 0 when it is absent) attached with MRP.

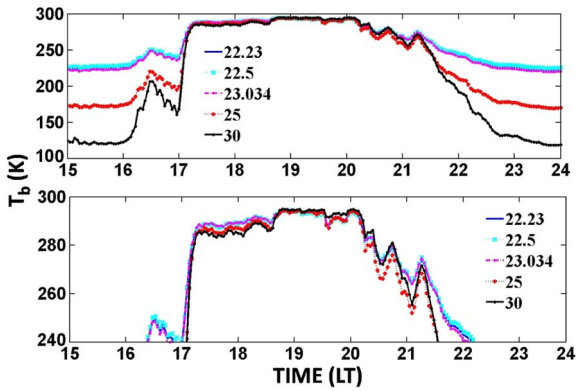

Fig. 3. T_b variability in K-band channels on November 25, 2013 (top panel). Zoomed figure showing the overlapping of 30 GHz channel after 19:00 LT (lower panel).

of MCSs during their genesis, evolution, and decay phases. A strong MCS event occurred on November 25, 2013, resulting in heavy accumulated rain of ∼70 mm from 18:00 to 22:30 Local Time (LT). The MRP multiangle observation permitted continuous monitoring of microphysical changes and propagation of system from land to sea, as shown in Fig. 2. The temporal evolution of the vertical distribution of relative humidity (RH) derived from radiometric observations at 15° east (over the land) and at 165° west (over the sea) is shown in the top and bottom panels, respectively. With November being the period of retreating monsoon, the prevailing humidity condition was very high in the altitude range of 2–4 km, as observed at 15:00 LT, even before the initiation of convection. After 17:00 h, RH building up started rapidly extending to altitudes above 6 km, indicating the initiation of convection (top panel). This buildup continued, and the system strengthened over the land by ∼19:00 LT, as large amount of humidity shoots up above 10 km. At the same time, the system also was propagating westward. The system evolved at ∼17:00 LT over the land (upper panel) and propagated over the sea, and it weakened by ∼21:00 LT and dissipated at ∼23:00 LT, as shown in the bottom panel. This MCS event lasted for ∼6 h over the MRP site, and it rained for ∼4 h.

3) Identification of CSs: A new methodology has been developed to identify convection based on the difference between the T_b values at 30- and 22.23 GHz channels. At frequencies below 50 GHz, the microwave signal emitted from a CS is essentially dominated by emission and absorption by cloud droplets and rain droplets and less affected by the presence of ice clouds. The cloud liquid water emission spectrum has no resonances in this frequency range, and absorption increases approximately with the second power of frequency [17]. The 30 GHz channel is more sensitive to liquid water content. The larger liquid water drops become more strongly absorbing, due to resonance effects within the drops, and also scatter the radiation.

The radiometric response at K-band channels to the CS that originated over the land on November 25, 2013 has been analyzed by examining the temporal variation of T_b (see Fig. 3). During the evolution of a CS, the atmospheric water molecules undergo phase changes, leading to energy exchanges, which can modify the thermal emission of the CS at different frequencies within the K-band. The T_b variations in the K-band channels during the evolution of the CS can be used to understand the microphysical properties. As shown in Fig. 3, during the prevailing background atmospheric condition at 15:00 LT, the K-band T_b values show significantly large differences between the water vapor resonant channel (22.3 GHz, higher T_b value of ∼225 K) and the window channel (30 GHz, lower T_b value of ∼100 K), which indicates the absence of clouds in the atmosphere. The difference between the T_b values of these two extreme channels $(\Delta T_{b(30-22)})$ is ∼−120 K at 15:00 LT, as shown in Fig. 3 (top panel). During the growth phase of the CS at ∼16:00 LT, the T_b value, for all K-band channels, increases continuously at different rates, and the differences between them decrease. As the CS matures, the differences among these channels become very small (as observed at ∼17:30 LT). The largest change in T_b occurred at 30 GHz, from ∼125 to ∼290 K, which indicates the formation of cloud liquid water. The minimum difference among all the T_b values indicates that, during the matured state of the CS, all the channels receive the thermal emissions which are emanating from almost within the same volume of atmosphere. The significant amount of liquid water droplets residing in the bottom region of the convective clouds scatter away the thermal emissions which are emanating from the higher altitude regions, resulting in almost the same T_b values for all the K-band channels. The zoomed-in view of T_b variations (bottom panel) shows that the T_b values at 30 GHz $(T_{b(30)})$, which were very low at ∼15:00 LT, increase with the strengthening of the system, and during the matured phase at ∼19:00 LT, the $T_{b(30)}$ crosses over the other water vapor channels, and the difference between these two channels becomes positive, which demarcates the core of the convection part from the rest of the MCS.

The concurrent measurements of R by the collocated disdrometer showed a homogeneous and less intense rain (2–5 mm · h^{-1}) from 18:10 to 19:00 LT, which was followed by the highly intense and variable rainfall (40–100 mm · h^{-1}) between 19:00 and 20:35 LT, with a short burst of intense rain (∼90 mm · h^{-1}) between ∼20:00 and 20:30, and followed by homogeneous and weak rain (∼2–5 mm · h^{-1}) from 20:45 to 22:30 LT. The present CS has a high degree of variability in its structure, as well as in rain rate. The T_b and concurrent rainfall measurements showed that, during stratiform precipitation, the water vapor emissions are high, i.e., $T_{b(22)} > T_{b(30)}$; the $\Delta T_{b(30-22)}$

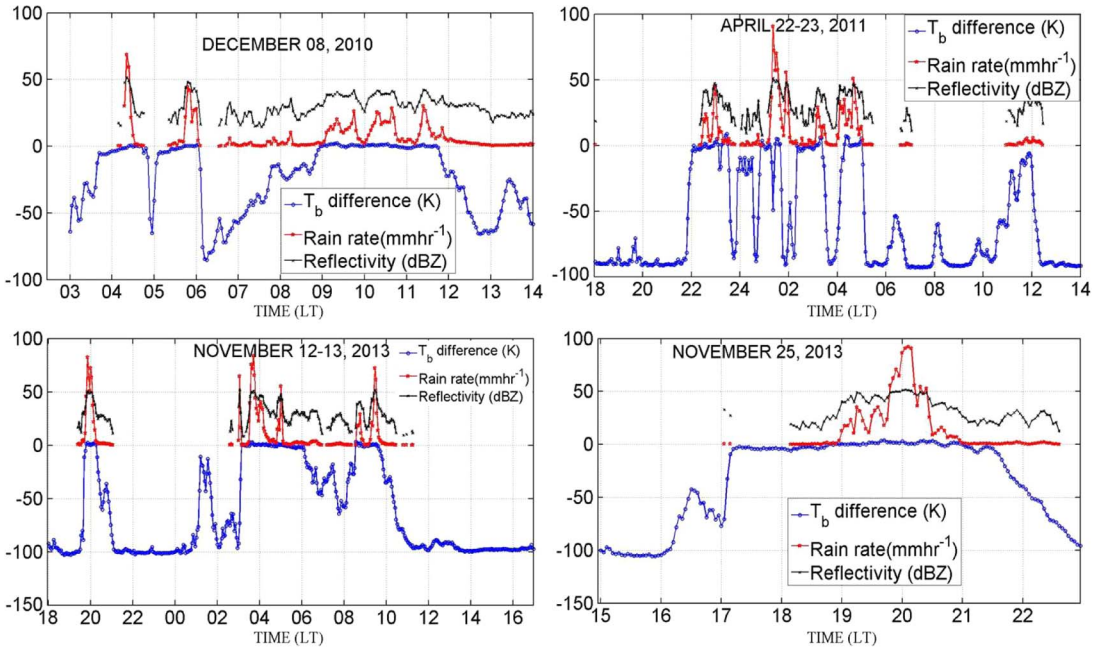

Fig. 4. T_b difference between the channels $(\Delta T_{b(30-22)})$ in kelvin (blue line), rain rate in mm $\cdot$ h^{-1} (red line), and reflectivity in dBZ (black line) for four MCS events (December 08, 2010; April 22–23, 2011; November 12–13; November 25, 2013).

becomes negative, and during convective precipitation time, $T_{b(22)} \leq T_{b(30)}$, and the $\Delta T_{b(30-22)}$ becomes zero or positive.

The cloud base temperature, which was measured by an IR radiometer attached to the MRP, indicated that the CBH decreased gradually from 5 to < 2 km, indicating the formation of cumulonimbus clouds, which is characterized with the liquid water as the dominant phase [18]. This is corroborated by the higher emission at 30 GHz due to the abundant hydrometeors present in the atmosphere, which went above the emissions from the rest of the channels. In view of the higher sensitivity of thermal emission at the 30 GHz channel (compared to the water vapor channel) to cloud liquid water, and considering the fact that tropical convective clouds can hold large amounts of liquid water, T_b differences between the 30- and 22.23 GHz channels $(\Delta T_{b(30-22)})$ have been used to characterize CSs over the site. The four typical MCSs that occurred over this site have been selected, whose $\Delta T_{b(30-22)}$, R, and Z data are analyzed in detail and shown in Fig. 4. During clear sky conditions, their $\Delta T_{b(30-22)}$ values are negative, and these become either zero or positive during the matured convective state, where Z (dBZ) also shows values above 38 dBZ, and R is also high, i.e., > 6 mm $\cdot$ h^{-1}, which confirm the MRP observations with the existing criteria.

The scatter plots between R and $\Delta\, T_{b(30-22)}$ (black bubbles) and Z and $\Delta T_{b(30-22)}$ (red open circles) are shown in Fig. 5. The plot between R and $\Delta T_{b(30-22)}$ shows the striking features of stratiform and CSs, with the former depicting low rain rates (< 12 mm $\cdot$ h^{-1}) over a large range (from -100 to -5 K) of $\Delta T_{b(30-22)}$, changing over to a near-delta-function-like association with heavy precipitation and almost zero or positive value of $\Delta T_{b(30-22)}$. $\Delta T_{b(30-22)}$ varies over a large range for reflectivity values below 38 dBZ, indicating the stratiform regime and large rain rates for reflectivity values above 38 dBZ, when $\Delta T_{b(30-22)} \geq 0$, signifying convective precipitation. For the mixed phase of convective and stratiform parts or the transition from the convective and stratiform region, $\Delta T_{b(30-22)}$ lies in between the limits [10]. In this region, convective and stratiform points overlap and become indistinguishable. The aforementioned analyses have brought out the effectiveness of the use of dual channels at 22.3 and 30 GHz to delineate the convective and stratiform regimes of MCSs.

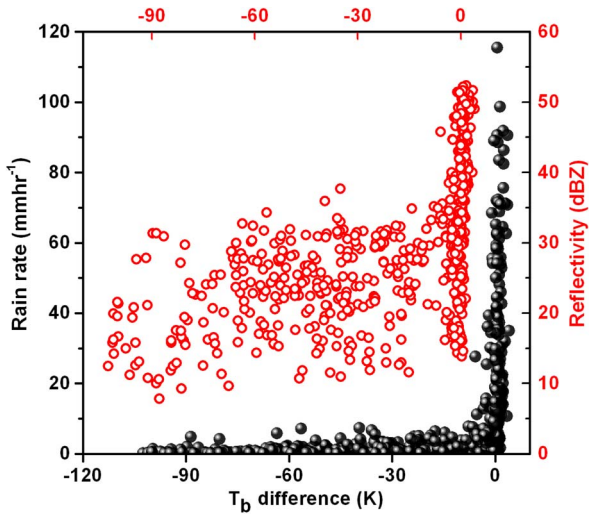

Fig. 5. Scatter plots between (left Y-axis) rain rate and (bottom X-axis) $\Delta T_{b(30-22)}$ (black filled circles) and between (right Y-axis) reflectivity (dBZ) and (top X-axis) $\Delta T_{b(30-22)}$ (red open circles) note that, for avoiding the overlapping of points, the top X-axis values have been shifted slightly from the bottom X-axis values, for the identified convective events.

4) Characterization of Tropical Convections: The aforementioned criterion to identify the convections has been employed to four years (2010–2013) of MRP observations, and 84 of such CSs were identified, which include both short-lived localized events and long-lived MCSs (44 CSs during pre-monsoon months and 40 systems during post-monsoon months), as shown in Fig. 6. The date of occurrence of convection and maximum R during each convective event are shown in Fig. 6 for pre-monsoon (first panel) and post-monsoon

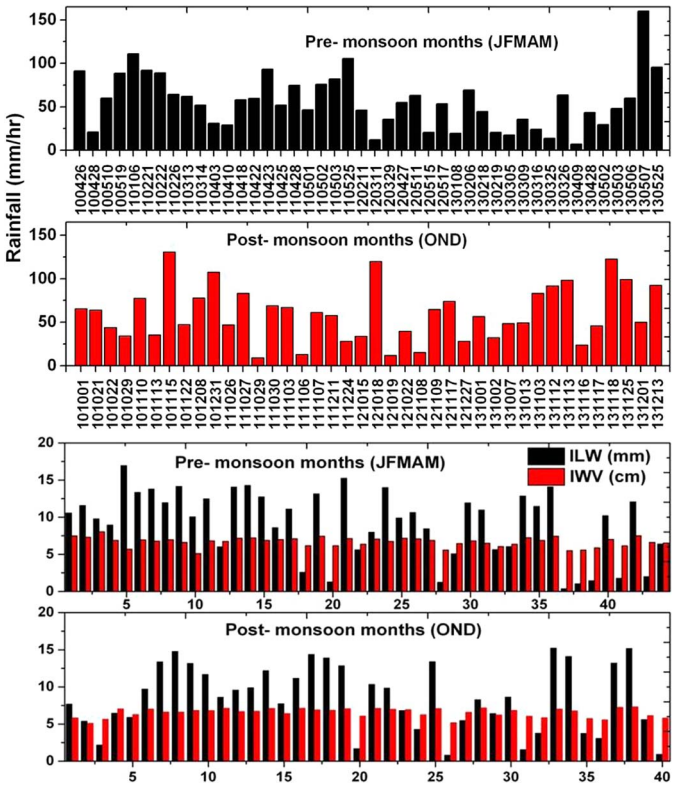

Fig. 6. Bar plot in the first two panels showing rainfall for 44 convective events identified during pre-monsoon months (January–May) (black) and for 40 convective events identified during post-monsoon months (October–December) (red) for the year 2010–2013. The X-axis corresponds to the date of occurrence of the individual events (in yymmdd format), and the Y-axis shows the accumulated rainfall during the event. The bar plots in the last two panels show IWV (red bars) and ILW (black bars) for convective events identified during pre- and post-monsoon months, respectively, and the X-axis corresponds to the day number of occurrence of individual events.

months (second panel) and the corresponding maximum values of integrated water vapor (IWV) and integrated liquid water (ILW) are shown in the third and fourth panels, respectively. R shows large variability from $\sim$6 to $\sim$150 mm $\cdot$ h^{-1}. IWV shows less variability ($\sim$2.5 cm), while ILW shows large variability ($\sim$15 mm), for these identified convections. In order to ascertain the accuracy of this methodology, the convective indexes, such as convective available potential energy (CAPE), K-index (KI), lifted index (LI), and total totals index (TT), are computed for each case to characterize the ability of the environment to support convection [19] and are shown in Fig. 7. All these events satisfy all the required stability conditions for convection: CAPE > 2000 J $\cdot$ kg^{-1}; KI > 35; LI > -2; and TT > 42.

This study also brings out that the occurrence of convection is more frequent during the April–May and October–November months because the surface temperatures (T_s) are higher (over continental and oceanic surfaces) during these periods over this region. The frequency of occurrence of thunderstorms per 1 °C rise in T_s is about 3–4 times higher in the near-equatorial latitude region than in the higher latitudes because the thermodynamics of moist convection is dependent on T_s [20]. It is also associated with the migration of the intertropical convergence zone (ITCZ) across this region, which is a zone of intense moist convective activity [21]. In the year 2013, the region experienced large MCSs and more frequent convection, particularly during the month of May and November, whereas

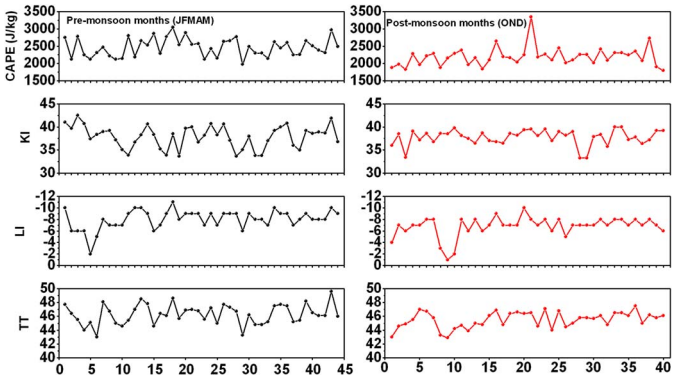

Fig. 7. Panels on the left show the stability indexes for 44 convective events during pre-monsoon months (January–May) (black), and those on the right side show these indexes for the 40 convective events during post-monsoon months (October–December) (red). The X-axis corresponds to the day number of occurrence of the individual events.

in the year 2012, the occurrence and strength of convective activities were less compared to the other years. The year 2012 was a deficit monsoon rainfall year, whereas year 2013 experienced heavy monsoon rainfall over the region [11]. The mean diurnal monthly patterns (not shown) of surface temperature (from meteorological sensors) indicate that the surface temperature during the pre-monsoon periods in the year 2013 shows slightly higher values (31.5 °C–32 °C) compared to the year 2012 ($\sim$30 °C). Hence, strong and frequent convection over the study site occurred during May 2013 and followed by a heavy monsoon rainfall, which is in accordance with the previous studies [20].

5) Diurnal Variation in the Occurrence of Convection: In order to understand the most conducive period for the occurrence of convections over the region, an analysis on the diurnal distribution of the occurrence of these CSs has been carried out. These results reveal that the frequency of occurrence of CSs is highest in the afternoon ($\sim$15:00 LT) and early-morning hours ($\sim$03:00 LT), as shown in Fig. 8. Most of the CS events occurring in the afternoon originate over the land, while those occurring in the early-morning hours have their origin over the sea. The genesis of convective activities over the land and the sea surfaces is mainly attributed to the differential heating of the two contrasting surfaces. The solar heating produces a late-afternoon maximum of convective available potential energy in the atmosphere, which supports late-afternoon moist convection and thunderstorms over the land area. The diurnal changes in differential heating between land and ocean surfaces in coastal areas produce diurnal phase patterns of surface wind divergence. This thermally driven land–ocean diurnal circulation may contribute to the general pattern of afternoon rainfall maxima over land areas and early-morning rainfall maxima over the adjacent oceans [22]. Similarly, over this tropical coastal region, the combined effect of thermally induced local circulations and air convergence results in afternoon convection over the land and early-morning events over the sea.

IV. Conclusion

The microphysical and thermodynamical characterization of different convective events, ranging from localized to mesoscale events, occurring over the tropical coastal station

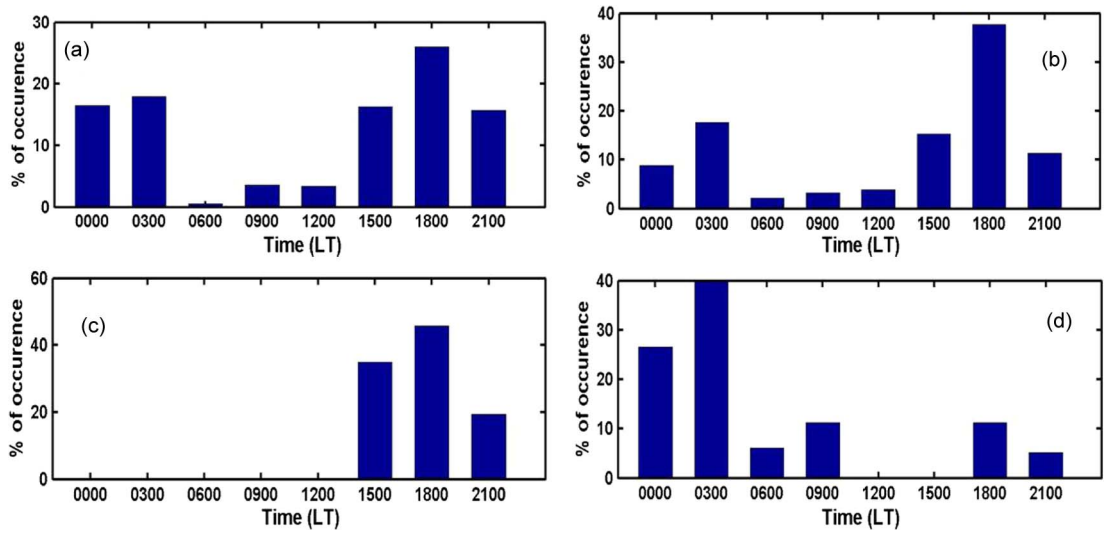

Fig. 8. (a) Frequency of occurrence of convective events during pre-monsoon months (January–May). (b) Frequency of occurrence of convective events during post-monsoon months (October–December). (c) Convective events originating over land. (d) Convective events originating over the sea.

TVM has been carried out using continuous observations of MRP for the period 2010–2013. A methodology to identify MCSs and to segregate the convective part by utilizing the T_b difference between 30- and 22.23 GHz channels is developed for ground-based radiometric measurements. $\Delta T_{b(30-22)} \geq 0$, is set as the criterion for distinguishing the convective events. The criterion has been verified based on the existing reflectivity and rain rate criteria deduced from collocated disdrometer measurements. Using the criterion, 84 convective events were identified and ascertained that all the identified events are CSs. The convections over the region are characterized on the basis of their frequency of occurrence and genesis. The occurrence of convection peaks during the pre-monsoon months of April and May and post-monsoon months of October and November. The occurrence of convection over this coastal station peaks in the afternoon and early-morning hours with genesis over the land and the sea, respectively. The radiometric technology developed here can provide information on water vapor and cloud liquid water, during the evolution of the CS, apart from the advanced information (now casting) of the genesis of CS, which is not possible from disdrometer or weather radar measurements. This study and the methodology developed for identifying convection and precipitation have significance in microwave (Ka- and W-band) satellite propagation characterization since CSs and precipitation are the major hindrance to satellite communication over the tropical region.

REFERENCES

[1] V. Ramanathan *et al.*, "Cloud-radiative forcing and climate: Results from the Earth Radiation Budget Experiment," *Science*, vol. 243, no. 4887, pp. 57–63, Jan. 1989.

[2] R. L. Grossman and O. Garcia, "The distribution of deep convection over ocean and land during the Asian summer monsoon," *J. Clim.*, vol. 3, no. 9, pp. 1032–1044, Sep. 1990.

[3] H. Riehl and J. S. Malkus, "On the heat balance in the equatorial trough zone," *Geophysica*, vol. 6, no. 3/4, pp. 503–538, 1958.

[4] E. J. Zipser, "Mesoscale and convective-scale downdrafts as distinct components of squall-line circulation," *Mon. Weather Rev.*, vol. 105, no. 12, pp. 1568–1589, Dec. 1977.

[5] R. A. Houze, "Observed structure of mesoscale convective systems and implications for large-scale heating," *Q. J. R. Meteorol. Soc.*, vol. 115, no. 487, pp. 425–461, Apr. 1989.

[6] A. Tokay and D. A. Short, "Evidence from tropical raindrop spectra of the origin of rain from stratiform versus convective clouds," *J. Appl. Meteorol.*, vol. 35, no. 3, pp. 355–371, Mar. 1996.

[7] C. R. Williams, W. L. Ecklund, and K. S. Gage, "Classification of precipitating clouds in the tropics using 915-MHz wind profiler," *J. Atmos. Ocean. Technol.*, vol. 12, no. 5, pp. 996–1012, Oct. 1995.

[8] J. F. Gamache and R. A. Houze, "Mesoscale air motions associated with a tropical squall line," *Mon. Weather Rev.*, vol. 110, no. 2, pp. 118–135, Feb. 1982.

[9] M. Fujiwara, "Raindrop size distribution from individual storms," *J. Atmos. Sci.*, vol. 22, no. 5, pp. 585–591, Sep. 1965.

[10] S. E. Yuter and R. A. Houze, "Measurements of raindrop size distributions over the Pacific warm pool and implications for Z-R relations," *J. Appl. Meteorol.*, vol. 36, no. 7, pp. 847–867, Jul. 1997.

[11] R. Renju, C. Suresh Raju, N. Mathew, T. Antony, and K. Krishna Moorthy, "Microwave radiometer observations of interannual water vapor variability and vertical structure over a tropical station," *J. Geophys. Res. Atmos.*, vol. 120, no. 9, pp. 4585–4599, May 2015.

[12] C. S. Raju, R. Renju, T. Antony, N. Mathew and K. Krishna Moorthy, "Microwave radiometric observation of a waterspout over coastal Arabian sea," *IEEE Geosci. Remote Sens. Lett.*, vol. 10, no. 5, pp. 1075–1079, Sep. 2013.

[13] Y. Han and E. R. Westwater, "Analysis and improvement of tipping calibration for ground based microwave radiometers," *IEEE Trans. Geosci. Remote Sens.*, vol. 38, no. 3, pp. 1260–1276, May 2000.

[14] U. Lohnert, S. Crewell, and C. Simmer, "An integrated approach toward retrieving physically consistent profiles of temperature, humidity, and cloud liquid water," *J. Appl. Meteor.*, vol. 43, no. 9, pp. 1295–1307, Sep. 2004.

[15] F. Solheim, J. Godwin, and R. Ware, "Passive ground-based remote sensing of atmospheric temperature, water vapor, and cloud liquid water profiles by a frequency synthesized microwave radiometer," *Meteorol. Z.*, vol. 7, pp. 370–376, Dec. 1998.

[16] N. V. P. Kirankumar and P. K. Kunhikrishnan, "Evaluation of performance of micro rain radar over the tropical coastal station Thumba (8.5° N, 76.9° E)," *Atmos. Res.*, vol. 134, pp. 56–63, Dec. 2013.

[17] C. Elachi, *Introduction to the Physics and Techniques of Remote Sensing.*, ser. Wiley Series in Remote Sensing. New York, NY, USA: Wiley, 1987.

[18] P. K. Wang, *Physics and Dynamics of Clouds and Precipitation*. Cambridge, U.K.: Cambridge Univ. Press, 2013.

[19] A. K. Showalter, "A stability index for thunderstorm forecasting," *Bull. Amer. Meteorol. Soc.*, vol. 34, no. 6, pp. 250–252, Jun. 1953.

[20] G. K. Manohar, S. S. Kandalgaonkar, and M. I. R. Tinmaker, "Thunderstorm activity over India and the Indian southwest monsoon," *J. Geophys. Res.*, vol. 104, no. D4, pp. 4169–4188, Feb. 1999.

[21] R. Markson, "Tropical convection, ionospheric potentials and global circuit variation," *Nature*, vol. 320, no. 6063, pp. 588–594, Apr. 1986.

[22] P. L. Silva Dias, J. P. Bonatti, and V. E. Kousky, "Diurnally forced tropical tropospheric circulation over South America," *Mon. Weather Rev.*, vol. 115, no. 8, pp. 1465–1478, Aug. 1987.

Authors' photographs and biographies not available at the time of publication.